Combustion Theory and Modelling
Publication details, including instructions for authors and subscription information:
http://www.tandfonline.com/loi/tctm20

Assessment of counterflow to measure laminar burning velocities using direct numerical simulations

Varun Mittal [a] , Heinz Pitsch [b] & Fokion Egolfopoulos [c]

[a] Department of Mechanical Engineering, Stanford University, CA, USA

[b] Institut für Technische Verbrennung, RWTH Aachen, Germany

[c] Department of Aerospace and Mechanical Engineering, University of Southern California, CA, USA

Available online: 17 Nov 2011

To cite this article: Varun Mittal, Heinz Pitsch & Fokion Egolfopoulos (2012): Assessment of counterflow to measure laminar burning velocities using direct numerical simulations, Combustion Theory and Modelling, 16:3, 419-433

To link to this article: http://dx.doi.org/10.1080/13647830.2011.631033

Combustion Theory and Modelling
Vol. 16, No. 3, 2012, 419–433

Assessment of counterflow to measure laminar burning velocities using direct numerical simulations

Varun Mittal,[a*] Heinz Pitsch[b] and Fokion Egolfopoulos[c]

[a]*Department of Mechanical Engineering, Stanford University, CA, USA;* [b]*Institut für Technische Verbrennung, RWTH Aachen, Germany;* [c]*Department of Aerospace and Mechanical Engineering, University of Southern California, CA, USA*

(*Received 2 June 2011; final version received 3 October 2011*)

The laminar burning velocity is a fundamental property that is extensively used in the study and modelling of premixed combustion processes. A counterflow flame configuration is commonly used to measure this quantity for different combustion systems. In this procedure, the burning velocities are typically measured at various low stretch conditions and the unstretched burning velocity is extrapolated from these measurements. This extrapolation is done assuming a theoretically one-dimensional system along the centre-line. We analyse the validity of this assumption by performing DNS studies with finite rate chemistry of the experimental counterflow configuration. The extrapolation process using one-dimensional computations is performed on the DNS data and the extrapolated value is compared to the computed laminar burning velocity for the chemical mechanism used. We show that the assumption works well if the nozzle exit velocity has a nearly top-hat profile. For non-uniform velocity profiles, it is shown that the temperature curvature at the centre-line becomes important. This effect cannot be captured by the one-dimensional formulation. Thus, experimental studies measuring laminar burning velocity need to ensure that the nozzle velocity profile is very close to uniform. The extrapolation to zero stretch using 1D counterflow simulations can be performed in different ways. Based on the results obtained in this paper, a simple and accurate extrapolation method is proposed.

Keywords: laminar burning velocity; counterflow configuration; burning velocity extrapolation; direct numerical simulation; premixed combustion

1. Introduction

Premixed combustion is important and needs to be understood in order to model modern combustion devices. Modelling this form of combustion is challenging due to the strong coupling between convection, diffusion, and chemistry. The laminar burning velocity is an important property that reflects this balance. It is used extensively to develop chemical mechanisms for various fuels that are then used to model both laminar and turbulent premixed combustion systems. Therefore, accurate experimental measurements of the burning velocity are essential. Two popular methods commonly used to obtain the burning velocity are a spherical flame setup [1] and a counterflow flame configuration [2]. In both these experiments, the flame has a non-zero stretch. Thus, the burning velocity measured is different from the unstretched laminar burning velocity and needs to be corrected. The

*Corresponding author. Email: mittal1@stanford.edu

ISSN: 1364-7830 print / 1741-3559 online

http://dx.doi.org/10.1080/13647830.2011.631033
http://www.tandfonline.com

counterflow configuration, for example, cannot measure the flame speed for very low strain rates, because the flames tend to flash back through the boundary layer when the stretch is too low. To overcome this problem, a commonly used technique is to measure the burning velocity at different strain rates. The unstretched burning velocity can then be obtained by using an extrapolation based on these values. Initial studies using these setups commonly used a linear extrapolation function based on an asymptotic analysis to obtain the unstretched burning velocity [3]. However, it was found that this relation does not hold over a wide range of stretch values and using this extrapolation generally leads to an over-prediction of the burning velocity. Further studies provided better nonlinear analytic relations between stretch and the burning velocity for a wider range of stretch values based on one-step chemistry [4]. To overcome the one-step chemistry limitation, Wang *et al*. [5] recently proposed using multi-step chemistry simulations to obtain the effect of the stretch on the burning velocity. This relation is then used to extrapolate the experimental burning velocity data to its unstretched value. Presently, it is not feasible to run many three-dimensional simulations of the experimental setup, which would be required to obtain the stretch dependence. Thus, the system was reduced to a one-dimensional formulation using a similarity assumption. The theoretical framework behind the assumption is discussed later.

While the procedure proposed by Wang *et al*. [5] seems to lead to a more accurate evaluation of the burning velocity, it is not clear if the one-dimensional framework can appropriately capture the flame dynamics under all the conditions realised in the experiment with the necessary accuracy. This is an essential requirement for the numerically calculated nonlinear relation used for the zero stretch extrapolation, to be valid. This work analyses the validity of this assumption using numerical simulations and it provides recommendations for properly extrapolating the burning velocities to zero stretch. Direct numerical simulations (DNS) of the counterflow experimental setup are carried out and the results are compared with those from the one-dimensional formulation. The flow conditions for this DNS study are laminar. First, some verification tests are shown between the two codes used for the DNS and the one-dimensional formulation to ensure consistency. Then, the one-dimensional and DNS results are compared for different strain rates. The extrapolated value of the burning velocity is then compared between the different formulations to quantify the effect of the one-dimensional assumption in the extrapolation procedure. Finally, a procedure is proposed for the zero-stretch evaluation of the laminar burning velocity.

2. One-dimensional counterflow configuration

For an axisymmetric flow in steady state, the low Mach number conservation equations for mass, x-momentum and energy in cylindrical coordinate system are

$$\frac{\partial}{\partial y}(\rho V) + \frac{1}{x}\frac{\partial}{\partial x}(\rho x U) = 0 \tag{1}$$

$$\rho U\frac{\partial U}{\partial x} + \rho V\frac{\partial U}{\partial y} = -\frac{\partial P}{\partial x} + \frac{1}{x}\frac{\partial}{\partial x}\left(x\mu\frac{\partial U}{\partial x}\right) + \frac{\partial}{\partial y}\left(\mu\frac{\partial U}{\partial y}\right) - \mu\frac{U}{x^2} + \frac{\partial U}{\partial x}\frac{\partial \mu}{\partial x} + \frac{\partial V}{\partial x}\frac{\partial \mu}{\partial y} \tag{2}$$

$$\rho U c_p \frac{dT}{dx} + \rho V c_p \frac{dT}{dy} = \frac{1}{x}\frac{\partial}{\partial x}\left(x\lambda\frac{\partial T}{\partial x}\right) + \frac{\partial}{\partial y}\left(\lambda\frac{\partial T}{\partial y}\right) - \sum_{i=1}^{N} h_i \dot{m}_i - \sum_{i=1}^{N} c_{p,i} j_{i,y} \frac{dT}{dy} - \sum_{i=1}^{N} c_{p,i} j_{i,x} \frac{dT}{dx}. \tag{3}$$

In these equations, the axial and radial coordinates are denoted as y and x, respectively. V is the axial velocity, U is the radial velocity, c_p is the mixture averaged specific heat capacity, λ is the thermal conductivity, $j_{i,k}$ is the diffusive flux of species i in direction k, h_i is the specific enthalpy of species i, and $\dot{m}_i$ is the chemical production rate of species i.

Three assumptions reduce the set of equations to a one-dimensional system. These assumptions have been used in earlier studies to study diffusion flames [6] and premixed flames [7]. The first assumption is that the radial velocity U varies linearly with radial distance close to the centre-line. Thus, it can be written in the form $U = G(y)x$, where G is a function of y only. The second assumption is that the pressure P has a similarity solution of the form

$$P = P_0 - \frac{1}{2}\left(P' x^2\right) + F(y). \tag{4}$$

Here, P_0 is the stagnation pressure and $F(y)$ is a function specifying the pressure variation in the axial direction. Finally, it is assumed that species and temperature do not have a radial dependence close to the centre-line. Using these assumptions, the governing equations (1)–(3) simplify to

$$\frac{\partial}{\partial y}(\rho V) + 2\rho G = 0 \tag{5}$$

$$\rho G^2 + \rho V \frac{dG}{dy} = P' + \frac{d}{dy}\left(\mu\frac{dG}{dy}\right) \tag{6}$$

$$\rho V c_p \frac{dT}{dy} = \frac{d}{dy}\left(\lambda\frac{dT}{dy}\right) - \sum_{i=1}^{N} h_i \dot{m}_i - \sum_{i=1}^{N} c_{p,i} j_{i,y} \frac{dT}{dy}. \tag{7}$$

Assuming a symmetric setup, the boundary conditions that need to be specified are

$$y \to 0 : V = V_{\text{nozzle}},\ G = (dU/dx)_{x=0,\ y=0},\ T = T_{\text{u}} \tag{8}$$

$$y \to L : V = -V_{\text{nozzle}},\ G = (dU/dx)_{x=0,\ y=L},\ T = T_{\text{u}}. \tag{9}$$

Here, L is the separation distance between the nozzles. The above conditions provide four boundary conditions for the continuity and the x-momentum equation, which over-constrains the system. Hence, the pressure parameter P' becomes an eigenvalue of the system. After obtaining P', the axial velocity profile V, along the centre-line, can be used to obtain the burning velocity at different stretch values.

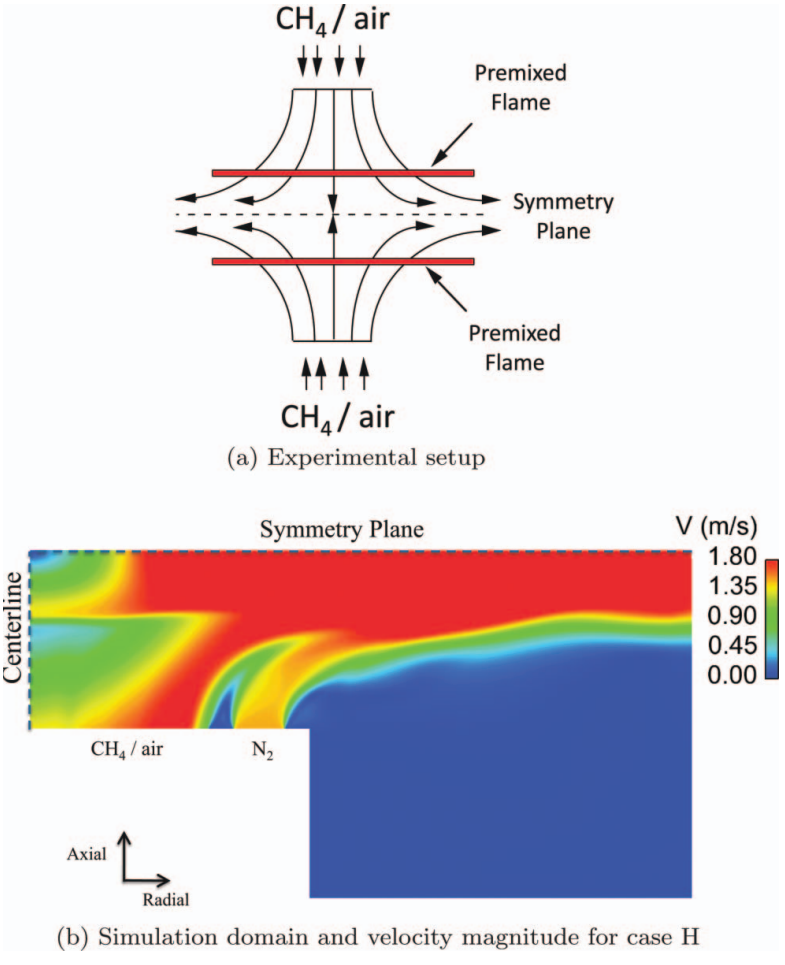

Figure 1. Experimental and simulation setup.

3. Setup

3.1. *Experimental setup*

The counterflow experimental setup studied is schematically shown in Figure 1. The details of the experimental methodology can be found in Ref. [8]. The fuel to be analysed is mixed with the oxidiser and fed through the central nozzle on both sides with a specified velocity. Two flames are formed away from the stagnation plane. Increasing the strain rate moves the flames farther away from the nozzle. For this study, a methane/air mixture with an equivalence ratio of 0.8 is used. A nitrogen co-flow is used to shield the flame in order to prevent external air entrainment effects. The diameter of the nozzle is 14 mm. The nozzle thickness is 1 mm, and the co-flow gap is 2 mm. Thus, the overall diameter of the tube is 20 mm. The distance between the nozzles is 14 mm. The mixtures have an initial temperature of 294 K. A contoured nozzle is used so that the velocity profile at the nozzle exit should be approximately uniform. However, it is found that the profile can deviate from a top-hat profile to various extents. This is an important difference that is highlighted later. For this study, an experimental condition with a strong non-uniformity was chosen to amplify the

effect in comparison with the ideal top-hat nozzle exit velocity profile case. Experimental studies typically have less non-uniformity in the nozzle velocity profile. The velocities of the fuel/air stream and the co-flow are varied to obtain different stretch rates. The three velocities used for this study are nominally 45 cm/s **(Case L)**, 97 cm/s **(Case M)**, and 145 cm/s **(Case H)**.

3.2. *Numerical setup*

To simulate the experimental setup, a high-order kinetic energy conserving code [9] is used. The code uses a second-order accurate semi-implicit Crank–Nicolson scheme for time advancement. The species are transported using a third-order accurate WENO scheme [10] to ensure boundedness of the scalars. Detailed multi-step finite-rate chemistry calculations are done with this code and therefore an accurate chemical mechanism can be used. The DVODE package [11] is used to advance chemistry implicitly. This code is referred to as the *DNS code* below. To solve the one-dimensional problem, the FlameMaster [12] code is used which has been extensively verified and tested. This code is referred to as the *1D code* in this study. In both codes, mixture averaged transport properties are used. The thermodynamic data is evaluated using NASA polynomials. Non-unity Lewis number effects and Soret diffusion effects are included in this study. GRI-MECH 3.0 [13] is used to model the methane chemistry in both codes.

3.3. *Laminar burning velocity calculation*

In this section, the experimental procedure for determining the laminar burning velocity from the measured data is explained. This is the same procedure as the one used in Ref. [5]. In the present study, this procedure will be tested using the DNS data as synthetic experimental data to obtain the unstretched burning velocity.

Experiments were done for different strain rates and the velocity profiles along the axis are measured. A typical profile, here obtained from the DNS, is shown in Figure 2. First, a reference velocity of the flame, $S_{u,ref}$, is defined as the velocity minimum just ahead of the flame. In the limit of zero stretch, $S_{u,ref}$ tends to the laminar burning velocity

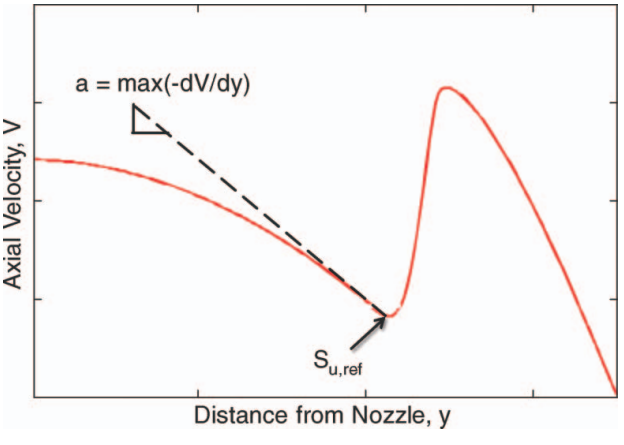

Figure 2. Sample axial velocity profile along the centre-line from the nozzle surface to the symmetry plane.

$S_{L,u}$. In addition, the nominal strain rate a is defined as the maximum velocity gradient $-dV/dy$ upstream of the minimum velocity point. These quantities are evaluated from the experimental velocity curves at different strain rates. An example for the resulting relation evaluated from the DNS is shown in Figure 7 below (filled squares), which will be further discussed later. The extrapolation of these values to zero stretch is assisted by results from one-dimensional simulations. For this, one-dimensional flames are computed at different strain rates (filled circles in Figure 7) and for the unstretched case (filled circle in Figure 7 at $a = 0\ \mathrm{s}^{-1}$). These data are fitted to obtain an extrapolation function (dashed line in Figure 7). Wang *et al*. [5] found that the shape of this function is invariant to small but finite changes in the chemical mechanism and transport coefficients used and is merely translated to higher or lower velocity values. This extrapolation function can then be translated vertically to match the experimental data to obtain the correct unstretched laminar burning velocity. For the case considered here, this leads to a substantial change of about 10% compared with the linear extrapolation.

4. Results

4.1. *Code verification*

To analyse the validity of the one-dimensional assumption, there must be no numerical differences between the results of the DNS code and the 1D code used in this study. First, to confirm that the chemistry integration is consistent between the codes, an autoignition problem is solved. The results for the temporal evolution of species and temperature are found to be identical between the codes. Then, to verify that the coupling between chemistry, convection, and diffusion is consistent between the codes, a laminar unstretched flame propagation problem is considered. The spatial profiles and the laminar burning velocity are found to be nearly identical between the codes. Therefore, any differences between the DNS modelling of the counterflow experiment and the 1D simulation results are due to the assumptions made for the one-dimensional formulation.

4.2. *Simulation setup*

To model the experimental setup, it is assumed that the setup is axisymmetric around the centre-line of the nozzle. This assumption is supported by the experimentally measured velocity fields, which are found to be axisymmetric. Also, symmetry is assumed around the stagnation plane of the setup. The resulting simulation domain is shown in Figure 1. Adequate grid resolution is used in the simulation to resolve the flame front correctly. The results are found to be invariant to increasing the grid resolution. Three different nozzle exit profiles (Cases L, M and H) measured from the experiment are used in the simulations as boundary conditions. Figure 3 shows these non-uniform nozzle exit profiles. The ratios of the maximum axial velocity to the centre-line axial velocity are 1.75, 1.45, and 1.37 for cases L, M, and H respectively. In order to analyse the effect of this deviation from a top-hat profile, three additional simulations are performed for the different strain rates using top-hat nozzle exit profiles. Those will be referred to as **Case** $\mathbf{L}_\mathrm{T}$, **Case** $\mathbf{M}_\mathrm{T}$, and **Case** $\mathbf{H}_\mathrm{T}$. A top-hat velocity profile is used for the nitrogen co-flow for all the cases.

Though the focus of this study is to analyse differences between the 1D results and the DNS results, DNS results are compared with the experiment qualitatively to verify that the simulation results are physically consistent. A comparison of the velocity field between the experiment and the simulation for the example of case H is shown in Figure 4. The agreement

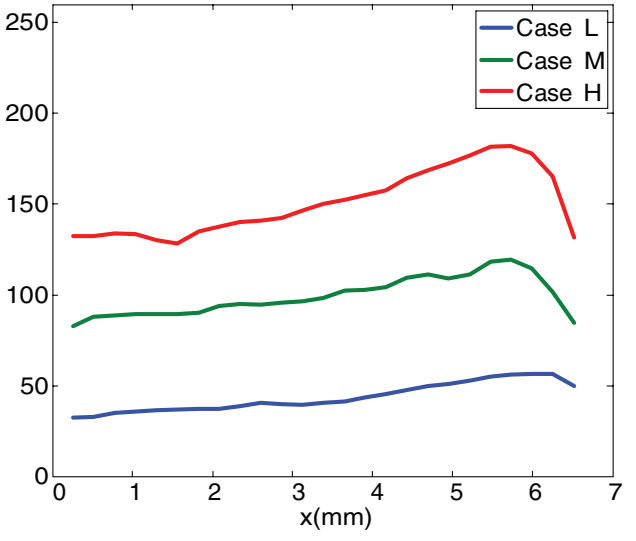

Figure 3. Axial velocity profile from experiment for different strain rate cases.

is quite good in both magnitude and qualitative features. Also, the location of the flame is predicted quite accurately. Both of the other cases studied here show similar comparison. Simulations also show that the co-flow shields the main flow adequately from the ambient air.

4.3. *1D vs. DNS comparison*

For the different cases, the velocity profiles at the centre-line are compared between the DNS and the 1D results. First, the results for the top-hat nozzle exit profile cases (top-hat cases) are compared and shown in Figure 5 for Case L_T. The comparison between the profiles is excellent and the flame sits at the same location for both formulations. Similar agreement is seen for all the cases. Consequently, the minimum velocity $S_{u,ref}$ and a between the DNS and 1D formulation are very similar. The values are shown in Table 1. It follows that the 1D assumption holds very well for a top-hat nozzle exit profile.

Next, the results are compared in Figure 6 (for case L) and Table 2 for the cases when the experimental profiles of the nozzle exit velocity are used as boundary conditions in the DNS simulations, and the experimentally observed dU/dx are used as boundary conditions in the

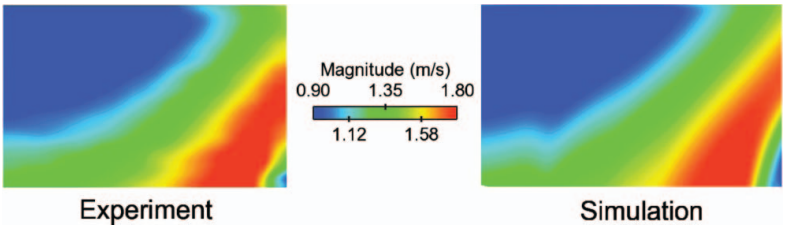

Figure 4. Comparison of the velocity field between the experiment (left) and the DNS (right) for case H.

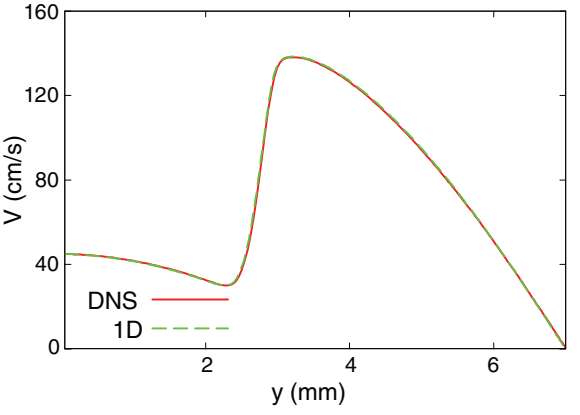

Figure 5. Comparison of the velocity profiles between DNS and the 1D formulation for case L_T.

1D simulations. The 1D results obtained using the exact experimental boundary conditions are shown under column 1D in Table 2. Though the flame sits at approximately the same location, the minimum velocity and the strain rate are quite different between the DNS and the 1D formulation as can be seen in Table 2. Similar differences are seen for all the cases. But, it is possible that the 1D results and the DNS results have the same relation between the strain and the burning velocity. To check this, another set of 1D simulations is performed where the strain rate is matched with the DNS data. If the same burning velocity is obtained as the DNS, then the '1D' simulations will be sufficient for obtaining the extrapolation. For these simulations, the inlet velocities are changed to match the nominal strain rate of the matching DNS case while keeping the separation distance constant. These results are presented in Table 2 under the '1D *a* adjusted' column. It is found that the minimum reference velocity is even more different when the strain rate is matched to the DNS results. In conclusion, it can be seen that the non-uniform nozzle velocity profile has a strong impact on the fluid dynamics and flame setup such that the one-dimensional assumption does not seem to hold as well as for the top-hat velocity profiles.

4.4. *Laminar burning velocity using DNS data*

Using the method outlined earlier, the unstretched burning velocity is extrapolated from the $S_{u,ref}$ values at the different strain rates obtained from the DNS to test the extrapolation procedure. The extrapolation function is calculated from the 1D formulation as described

Table 1. Comparison between the ID formulation and the DNS with top-hat nozzle exit profile.

	$S_{u,ref}$ (cm/s)		a (1/s)	
Case	DNS	1D	DNS	1D
Case L_T	30.02	30.00	115.7	115.4
Case M_T	34.33	34.39	276.4	277.5
Case H_T	37.28	37.59	411.9	412.3

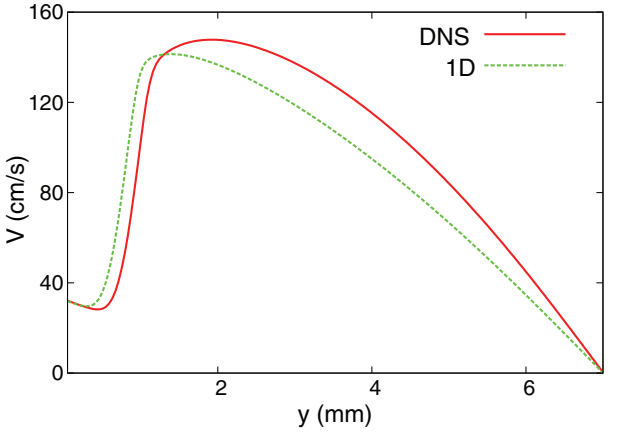

Figure 6. Comparison of the velocity profiles between DNS and the 1D formulation for case L.

earlier. If the nozzle separation distance is kept constant in the 1D simulations, the strain rate can only be lowered until heat losses to the burner become relevant. After a sufficient number of 1D solutions is obtained, the extrapolation function is obtained by vertically shifting the 1D results in Figure 7 to best match the DNS data. This procedure is shown in Figures 7 and 9 (below) for the cases with the top-hat inlet velocity profiles and the cases using the notably non-uniform experimental velocity inlet profiles, respectively. Both figures show the 1D solutions for varying strain rates including the computed value for the unstretched case, the fit to these data, the data from the DNS serving as pseudo-experimental data, and the extrapolation function that is obtained by vertically shifting the fit to match the DNS data. Figure 8 also shows the experimental data, which in terms of the stretch dependence of the burning velocity, is in quite good agreement with the DNS. A laminar burning velocity follows for each set of cases as the value at zero stretch of the translated extrapolation function. The laminar burning velocities obtained along with the correct value obtained from the solution of the one-dimensional laminar unstretched flame equations are shown in Table 3.

The extrapolated laminar burning velocity based on data from the cases with top-hat velocity profile (Case L_T, Case M_T and Case H_T) is very close to the expected laminar burning velocity. However, the laminar burning velocity obtained by extrapolating data from the cases using the experimental inlet velocity profiles (Case L, Case M and Case H) is significantly different from the expected value. This indicates that the 1D assumption

Table 2. Comparison between DNS and ID formulation for experimental nozzle velocity exit profile.

	$S_{u,ref}$ (cm/s)			a (1/s)	
Case	DNS	1D	1D α adjusted	DNS	1D
Case L	28.22	29.62	29.63	129.12	128.58
Case M	30.14	31.85	32.43	232.65	212.27
Case H	33.15	33.79	34.38	310.25	285.25

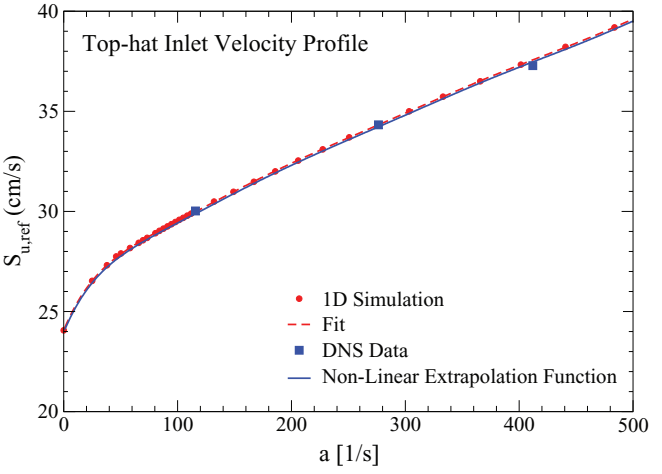

Figure 7. Relation between $S_{u,ref}$ and a for top-hat nozzle exit velocity profile cases (Case L_T, Case M_T and Case H_T).

is not valid and leads to substantial errors in the nonlinear extrapolation when notable non-uniformities of the nozzle exit velocity profile are present.

5. Analysis of the one-dimensional assumptions

To identify the reason for the discrepancy in the laminar burning velocity obtained for the non-uniform nozzle profile cases, the validity of the assumptions inherent in the one-dimensional formulation is analysed for cases L and H.

The different assumptions made were explained earlier in Section 2. First, it is assumed in the one-dimensional formulation that the radial velocity is linearly dependent on the radius for the region close to the centre-line. This assumption is found to be valid for all of the cases. The next assumption made is that the pressure P follows a similarity solution

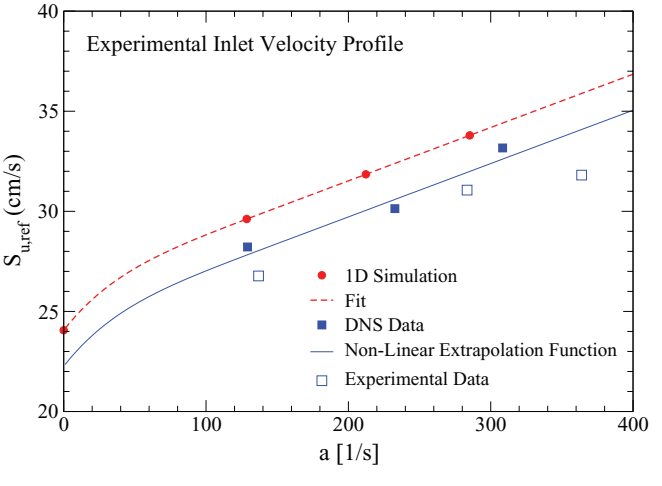

Figure 8. Relation between $S_{u,ref}$ and a for experimental nozzle exit velocity profile cases (Case L, Case M and Case H).

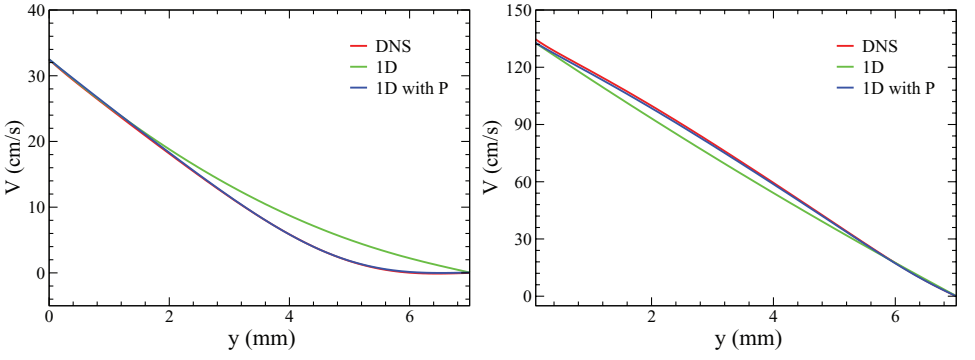

(a) Case L (b) Case H

Figure 9. Comparison of the velocity profiles between DNS and the 1D formulation for experimental nozzle velocity profiles for non-reacting simulations. The 1D represents runs with the original formulation. 1D P represents simulations when the non-uniform pressure curvature is included from the DNS.

of the form shown in Equation (4). Consequently, the radial curvature of P is assumed to be constant in the axial direction and equal to $-P'$. However, based on the DNS results, this radial pressure curvature is actually found to vary significantly in the axial direction. To check if this is the reason for the discrepancy, the functional form of P is modified to include the pressure curvature profile from the DNS as

$$P = P_o - \frac{1}{2}\left(P' f(y) x^2\right) + F(y), \tag{10}$$

where $f(y)$ is obtained from the DNS as $P' f(y) = -\partial^2 P/\partial x^2$. This dependence is included in simulations of both non-reacting and reacting cases. For the non-reacting cases, the inclusion of the $\partial^2 P/\partial x^2$ from the DNS leads to excellent agreement between the DNS and the 1D results. The results can be seen in Figure 9. When applied for the reacting cases, however, discrepancies still remain. Figure 10 shows the relation of the burning velocity to stretch in the linear region with and without consideration of the non-uniform pressure curvature. Although the velocity profile shown in Figure 9 is strongly improved, the values of the burning velocity are different for the two cases and the relation with the strain rate is completely unchanged. Thus, the discrepancy in the extrapolated burning velocity is not due to the non-uniform radial pressure curvature.

Another major assumption made in the one-dimensional formulation is that the radial curvature of species and temperature is negligible close to the centre-line. However, it is found from the DNS data that these curvatures are actually quite significant near the flame

Table 3. Extrapolated laminar burning velocity for different velocity profiles.

Case	$S_{L,u}$ (cm/s)
Case L, Case M, Case H	22.27
Case L_T, Case M_T, Case H_T	24.06
Correct value	24.06

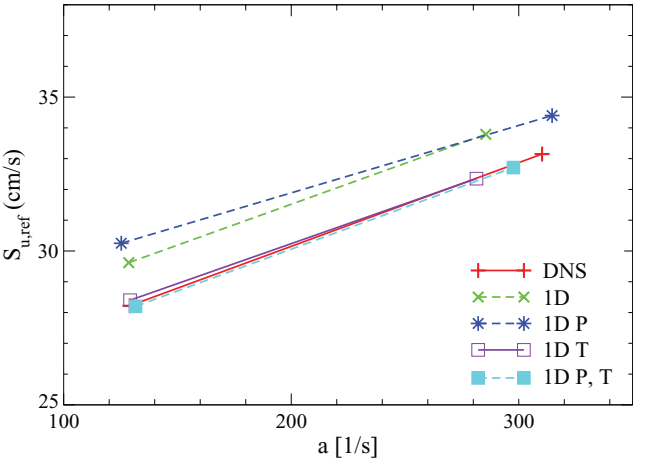

Figure 10. Relation between $S_{u,ref}$ and a for experimental nozzle velocity profile cases when different curvature effects are included. 1D represents runs with the original one-dimensional formulation. 1D P represents simulations when the non-uniform pressure curvature is included from the DNS. 1D T provides data for the runs when the radial temperature curvature is included from the DNS. Similarly, 1D P,T represents runs when the non-uniform radial curvature of temperature and pressure is included.

for all the non-uniform nozzle velocity cases. The effect of this assumption is tested by including the actual non-uniform temperature curvature in the energy equation (3). The modified equation after including the radial temperature curvature effects is

$$\rho V c_p \frac{dT}{dy} = \frac{d}{dy}\left(\lambda \frac{dT}{dy}\right) + \left[\frac{d}{dx}\left(\lambda \frac{dT}{dx}\right)\right]_{DNS} - \sum_{i=1}^{N} h_i \dot{m}_i - \sum_{i=1}^{N} c_{p,i} j_{i,y} \frac{dT}{dy}. \quad (11)$$

Here, the radial curvature term is directly computed from the DNS data along the centre-line. Similarly, the effect of the species radial curvature can also be included in the species transport equations along the centre-line. Comparisons are made after including different combinations of these curvature effects on the strain and burning velocity relation to find out the minimum subset of terms required to obtain the correct relation. It is found that including just the pressure and temperature curvature leads to almost identical strain rates and burning velocities between the DNS and one-dimensional simulations. This can be seen in Figure 10. However, including the temperature curvature effect alone after neglecting the pressure and species curvature, is sufficient to obtain a consistent burning velocity dependence on strain between the two formulations as is shown in Figure 10. After including these one-dimensional results with radial temperature curvature and the unstretched burning velocity, a new extrapolation function can be obtained. For the cases considered, this function is a nearly linear function but this is fortuitous and does not represent a general trend. Using this extrapolation function leads to the correct unstretched burning velocity when it is used to extrapolate the DNS results.

Thus, it is important to account for radial temperature curvature effects when using a nozzle velocity profile, which is not exactly top-hat. Neglecting these effects leads to an incorrect extrapolated unstretched burning velocity.

6. Discussion

As a result here, it is found that the nonlinear extrapolation leads to very accurate results, if the nozzle exit velocities have a top-hat profile. For strongly non-uniform inlet velocities, the assumptions leading to the 1D formulation used in the nonlinear extrapolation are not satisfied. In particular, the non-zero second derivative of the temperature in the radial direction is of importance, which is neglected in the 1D formulation. This radial temperature curvature is induced by the non-uniform velocity profile. This leads to a systematic error in the evaluation of the laminar burning velocity, which is of the same order as the error in the prediction of the velocity in the linear region. Hence, for performing correctly the nonlinear extrapolation, there are three options. First, uniform inlet velocity profiles have to be ensured. The second option is to measure the second derivative of the temperature in the radial direction along the centre-line and impose it in the simulations. While this quantity is non-zero only within the flame, it might not be measurable in a straightforward manner. The third option is to perform at least one multi-dimensional simulation with the correct inlet velocity profile to determine the systematic shift introduced by the non-top-hat velocity profile. This option also might not be straightforward, especially when large chemical mechanisms have to be considered.

Apart from this potential systematic error, it is here further recommended to apply the extrapolation in a slightly different way. While this revised procedure does not remove the error associated with radial temperature curvature effects, it attempts to simplify the extrapolation procedure. It is obvious from Figures 7 and 8 that there exists a linear relation between the reference burning velocity $S_{\mathrm{u,ref}}$ and the nominal strain rate at high enough strain rates. This relation is assumed to be correctly predicted by the simulations if the chemical mechanism used is consistent. Apart from this linear region, the nonlinear extrapolation function also considers the nonlinear part of the function at low strain rates and the computed value of the unstretched laminar burning velocity $S^c_{L,u}$. From all this, the most trustworthy and robust parts are first of all the $S^c_{L,u}$ value, which is exact for the given mechanism, and further the linear part of the relation, which typically occurs over a large range. The exact shape of the nonlinear part of the curve is not important, as long as the linear part and the value of $S^c_{L,u}$ are known. However, the procedure described earlier develops a function that fits the entire range of burning velocities well. Note that that procedure does not ensure that the fitting function also matches the $S^c_{L,u}$ value. A more reliable velocity extrapolation procedure therefore relies only on the linear region and the value of $S^c_{L,u}$. For this, 1D stretched flame solutions are first computed to identify the linear regime. A linear fit, $S_{\mathrm{u,ref,1D}}(a) = b_{\mathrm{1D}}a + c_{\mathrm{1D}}$, is then used to obtain b_{1D} and c_{1D} from the one-dimensional solutions in the linear regime. Using then the same value for the linear slope b_{1D} to fit the experimental data for the burning velocities relation with strain values, a linear fit, $S_{\mathrm{u,ref,exp}}(a) = b_{\mathrm{1D}}a + c_{\mathrm{EXP}}$, provides the value of the linear intercept, c_{EXP}. The extrapolated burning velocity can then be computed using the difference of the two intercepts and the computed unstretched laminar burning velocity as

$$S_{L,u} = S^c_{L,u} - (c_{\mathrm{1D}} - c_{\mathrm{EXP}}). \tag{12}$$

This procedure is shown in Figure 11. It is important here that only the computed laminar burning velocity value and the linear slope are used to correct the measured values for zero stretch. For this, the linear slope could also be evaluated from the experimental data. However, both should be consistent to within the experimental accuracy and the evaluation from the computed data should be more accurate, because a wider linear region

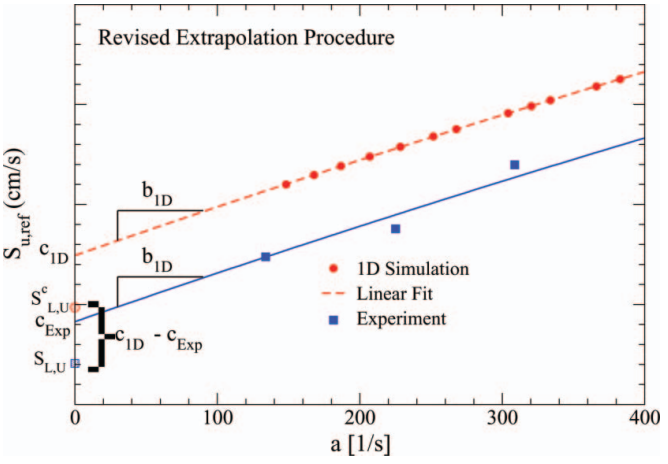

Figure 11. Illustration of the revised extrapolation procedure.

is available. If the slopes of the experimental and computed linear region are not consistent, the mechanism used for the computations might not be accurate enough and this procedure cannot be used.

7. Conclusions

The validity of the one-dimensional assumption and the procedure used to extrapolate strained burning velocities from a counterflow configuration to determine the unstretched laminar burning velocity are assessed. Direct numerical simulations of the experimental setup are performed and the results are compared with a 1D similarity formulation. Three different strain rates are compared between the experiment and the DNS. It is found that the velocity fields are similar, and thus, the simulation adequately represents the experimental setup for the purpose of the present study. Results from the DNS are then compared with results from the 1D formulation. Very good agreement demonstrating the validity of the one-dimensional assumption is found if a top-hat nozzle exit velocity profile is used. However, it is found that the nonlinear extrapolation function, which is based on results from a one-dimensional formulation, is not as good, if strong non-uniformities in the nozzle exit velocity are present. This difference is found to be caused by non-zero radial second derivatives in the centre-line temperature profile due to the non-uniform velocity. Thus, experimental studies measuring laminar burning velocity need to ensure that the nozzle velocity profile is very close to uniform. If that is not feasible, the radial temperature curvature profile needs to be estimated and considered in the 1D simulations in order to obtain the correct laminar burning velocity. In addition, a slightly revised, more robust extrapolation method is proposed here, where only the computed burning velocities of the linear regime and the unstretched value are used.

References

[1] D. Bradley, R.A. Hicks, M. Lawes, C.G.W. Sheppard, and R. Woolley, *The measurement of laminar burning velocities and Markstein numbers for iso-octane-air and iso-octane-n-heptane-air mixtures at elevated temperatures and pressures in an explosion bomb*, Combust. Flame 115 (1998), pp. 126–144.

[2] F. Egolfopoulos, D. Zhu, and C. Law, *Experimental and numerical determination of laminar flame speeds: Mixtures of C2-hydrocarbons with oxygen and nitrogen*, Proc. Combust. Inst. 23 (1990), pp. 471–478.
[3] C. Law, D. Zhu, and G. Yu., *Propagation and extinction of stretched premixed flames*, Proc. Combust. Inst. 21 (1986), pp. 1419–1426.
[4] J. Tien and M. Matalon, *On the burning velocity of stretched flames*, Combust. Flame 84 (1991), pp. 238–248.
[5] Y. Wang, A. Holley, C. Ji, F. Egolfopoulos, T. Tsotsis, and H. Curran, *Propagation and extinction of premixed dimethyl-ether/air flames*, Proc. Combust. Inst. 32 (2009), pp. 1035–1042.
[6] L. Krishnamurthy, F. Williams, and K. Seshadri, *Asymptotic theory of diffusion-flame extinction in the stagnation-point boundary layer*, Combust. Flame 26 (1976), pp. 363–377.
[7] R.J. Kee, J.A. Miller, G.H. Evans, and G. Dixon-Lewis, *A computational model of the structure and extinction of strained, opposed flow, premixed methane–air flames*, Symposium (International) on Combustion 22 (1989), pp. 1479–1494.
[8] C. Ji, E. Dames, Y. Wang, H. Wang, and F. Egolfopoulos, *Propagation and extinction of premixed C5-C12 n-alkane flames*, Combust. Flame 157(2) (2009), pp. 277–287.
[9] O. Desjardins, G. Blanquart, G. Balarac, and H. Pitsch, *High order conservative finite difference scheme for variable density low Mach number turbulent flows*, J. Comput. Phys. 227 (2008), pp. 7125–7159.
[10] X. Liu, S. Osher, and T. Chan, *Weighted essentially non-oscillatory schemes*, J. Comput. Phys. 115 (1995), pp. 200–212.
[11] P. Brown, G. Byrne, and A. Hindmarsh, *VODE, A variable-coefficient ODE solver*, SIAM J. Sci. Statist. Comput. 10 (1989), pp. 1038–1051.
[12] H. Pitsch, H. Barths, and N. Peters, *Three-dimensional modeling of NOx and soot formation in DI-diesel engines using detailed chemistry based on the interactive flamelet approach*, SAE Paper 962057 (1996).
[13] G.P. Smith, D.M. Golden, M. Frenklach, N.W. Moriarty, B. Eiteneer, M. Goldenberg, C.T. Bowman, R.K. Hanson, S. Song, W.C.G. Jr., V.V. Lissianski, and Z. Qin, *GRI-Mech 3.0*, available at: http://www.me.berkeley.edu/gri_mech/ (accessed 3rd October 2011).